

3-21-2019

Sharpening land use maps and predicting the trends of land use change using high resolution airborne image: A geostatistical approach

Bo Yang

San Jose State University, bo.yang02@sjsu.edu

Susanna T.Y. Tong

University of Cincinnati

Rong Fan

University of Cincinnati

Follow this and additional works at: https://scholarworks.sjsu.edu/faculty_rsca

Recommended Citation

Bo Yang, Susanna T.Y. Tong, and Rong Fan. "Sharpening land use maps and predicting the trends of land use change using high resolution airborne image: A geostatistical approach" *International Journal of Applied Earth Observation and Geoinformation* (2019): 141-152. <https://doi.org/10.1016/j.jag.2019.03.010>

This Article is brought to you for free and open access by SJSU ScholarWorks. It has been accepted for inclusion in Faculty Research, Scholarly, and Creative Activity by an authorized administrator of SJSU ScholarWorks. For more information, please contact scholarworks@sjsu.edu.



Sharpening land use maps and predicting the trends of land use change using high resolution airborne image: A geostatistical approach

Bo Yang^{a,b}, Susanna T.Y. Tong^{a,*}, Rong Fan^a

^a Department of Geography, University of Cincinnati, Cincinnati, OH 45221, USA

^b Department of Sociology, University of Central Florida, Orlando, FL 32816, USA

ARTICLE INFO

Keywords:

Land use
Change detection
Sharpening algorithm
Multispectral
Classification

ABSTRACT

High quality land use/land cover (LULC) data with fine spatial resolution and frequent temporal coverage are indispensable for revealing detail information of the Earth's surface, characterizing LULC of the area, predicting the plausible land use changes, and assessing the viability and impacts of any development plans. While airborne imagery has high spatial resolution, it only provides limited temporal coverage over time. The LULC data from historical remote sensing images, such as those from Landsat, have frequent coverages over a long temporal period, but their spatial resolutions are low.

This paper presents a spatio-temporal Cokriging method to sharpen LULC data and predict the trends of land use change. A set of time-series coarse resolution LULC maps and one frame of high spatial resolution airborne imagery of the Upper Mill Creek Watershed were used to illustrate the utility of our method. By explicitly describing the spatio-temporal dependence within and between different datasets, modelling the Anderson classification codes using spatial, temporal, and cross-covariance structures, and transforming the Anderson integer classification code to class probability, our method was able to resolve the differences between multi-source spatio-temporal LULC data, generate maps with sharpened and detailed land features, characterize the spatial and temporal LULC changes, reveal the trend of LULC change, and create a quality dataset invaluable for monitoring, assessing, and modelling LULC changes.

1. Introduction

The terrestrial features on the Earth's surface are extremely diversified, and they are changing rapidly, particularly in urbanized regions. To better observe the features of land use and land cover (LULC), capture a more realistic and detailed picture of its patterns, and monitor its changes over time, one needs spatio-temporal (ST) data with fine spatial and temporal resolutions (Fan et al., 2017; Sun et al., 2016; Tong and Naramngam, 2007). Nonetheless, many LULC data have either high temporal frequency or high spatial resolution, but not both. The U.S. Geological Survey (USGS) National Land Cover Database (NLCD), for example, has frequent and extended temporal coverage, but a low spatial resolution of 30 m. Therefore, a technical challenge is to derive a spatial data handling method that can produce images at both high spatial resolution and high temporal frequency.

Numerous image-sharpening methods have been developed whereby an image from a fine resolution panchromatic band is used to increase the spatial resolution of another data source. Traditional methods include wavelet transformation (Yocky, 1996) and Gram-

Schmidt method (Ling et al., 1986). Geostatistical methods, such as inverse distance weighted method (IDW), have also been applied to spatial data fusion and sharpening (Kyriakidis and Journel, 1999). Recently, Jeganathan et al. (2011) developed a thermal image sharpening algorithm and Gilbertson et al. (2017) proposed a multi-temporal imagery sharpening model. While these methods can improve the spatial resolution of a dataset, they are not suitable to perform spatio-temporal data sharpening, because they model only one point in time and do not address the quantitative temporal changes induced by phenology and seasonality. Other researchers, such as Snepvangers et al. (2003), used two kriging methods (a spatio-temporal ordinary kriging and a spatio-temporal kriging with an external drift). Nevertheless, their kriging methods were not designed to deal with raster datasets created from satellite observations. Atkinson et al. (2008) developed a downscaling Cokriging method by using a coarse resolution image as a primary variable and a higher spatial resolution image at a different spectral band as a co-variable. Although spatial covariance and cross-covariance structures between primary and secondary images were taken into account in their study, the downscaling Cokriging

* Corresponding author.

E-mail addresses: Bo.Yang@ucf.edu (B. Yang), susanna.tong@ucf.edu (S.T.Y. Tong), fanrg@mail.uc.edu (R. Fan).

method did not model the time dimension. Therefore, their method is still unable to perform spatio-temporal data sharpening. Liu et al. (2008) used dominant driving factors, such as encroachment of urban development, to model LULC change. While their method works well, it is not suitable for a region that lacks data on the dominant factors. van der Sande et al. (2003) derived a segmentation-based approach to improve LULC mapping for flood assessments, but their approach is not suitable for LULC change detection analyses because it only uses spatial information to depict the LULC pattern. Verhoeve and Wulf (2002) also proposed to use a linear optimization algorithm, which utilizes a weighted function to address spectral differences between multi-sensors data. However, they adopted a heuristic approach and arbitrarily assigned fraction values to the sub-pixel of the LULC data. The effectiveness and accuracy of this method are therefore limited.

This paper proposes a new spatio-temporal Cokriging (ST-Cokriging) technique by extending traditional Cokriging from a spatial domain to a space-time domain. This is the first attempt to sharpen classification maps via a geostatistical approach. Our method is capable of assimilating images of temporally frequent but coarse spatial resolution with images of fine spatial resolution but a sparse temporal coverage. Its algorithm takes into account the spatial and temporal covariance and cross-covariance structures. The validation results and accuracy assessments showed that our multi-scale spatio-temporal sharpening technique provided reliable LULC predictions with more detail.

Moreover, previous LULC change detection methods, such as those by Liu et al. (2008), were designed to use the image spectral values rather than the classification codes. Only a few were focused on establishing the quantitative connection and transmission between LULC classes (van der Sande et al., 2003). However, the coded classes are different from spectral values. To calculate the spatio-temporal change probabilities, the relationships between nested classes need to be considered, while spatial, temporal, and spatio-temporal independence between and within multi-source data need to be modelled appropriately. In this research, our sharpening algorithm was designed specifically for systematic classification values, such as the LULC Anderson classification codes (Anderson et al., 1976). As the Anderson codes are transmittable and generalizable, the changing trend and the rate of the temporal changes can be calculated; as such, the sharpened maps are invaluable for future land development. To make it easier for other users, our sharpening algorithm is included in a software package. Through the user interface for batch processing, users can apply it to other study regions even with a different spatial scale.

2. Methodology

2.1. Sharpening method for Anderson classification

The Anderson classification method is commonly used to classify datasets, including NLCD LULC (Anderson et al., 1976; MRLC (Multi-Resolution Land Characteristics Consortium), 2017). By naming classes according to accepted terminology, coding information so that it can be transmitted, and allowing inductive generalizations, it satisfies the three major attributes of classification (Grigg, 1965). To allow cross-categories comparison, its nested class codes are represented by two digits (the first digit represents the land use category, and the second digit shows the different levels within that land use category; see Table 1). For instance, when comparing the categories of deciduous forest with shrub/scrub and high density developed area, the difference between deciduous forest (41) and shrub/scrub (52) is smaller than the difference between deciduous forest (41) and high intensity developed area (24), thereby reflecting that the class category of deciduous forest is more similar to shrub/scrub (52) than to high intensity developed area (24). The order of the class code also represents the trend of LULC change; for example, in the category of developed area, open space is coded as 21, low intensity developed area is 22, medium intensity is 23,

Table 1
Anderson land cover classification system for NLCD data.

Category	Class	Code
Water	Open Water	11
	Perennial Ice/Snow	12
Developed	Developed, Open Space	21
	Developed, Low Intensity	22
	Developed, Medium Intensity	23
	Developed High Intensity	24
Barren Forest	Barren Land (Rock/Sand/Clay)	31
	Deciduous Forest	41
	Evergreen Forest	42
Shrubland	Mixed Forest	43
	Dwarf Scrub	51
Herbaceous	Shrub/Scrub	52
	Grassland/Herbaceous	71
	Sedge/Herbaceous	72
	Lichens	73
Planted/Cultivated	Moss	74
	Pasture/Hay	81
	Cultivated Crops	82
Wetlands	Woody Wetlands	90
	Emergent Herbaceous Wetlands	95

and high intensity is 24. With the classes coded in integers, the class order enables the calculation of the probability of change between two adjacent class codes. As shown in Fig. 1, the decimal between the classes could be used to show the temporal correlation between the time-series LULC data and calculate the LULC changing probability. As an illustration, the value of 21.73, which represents developed area, means that there is a 73% probability for the object to be in the class of low intensity development (Anderson class code 22). By representing not only the possibility of an object that will fall in a specific LULC class, but also the trend of transformation in the spatio-temporal context, the LULC probability is useful for detecting the spatio-temporal change of LULC.

2.2. Spatio-temporal extended Cokriging

Cokriging is an extension of a kriging system to more than one variable in the space domain with one primary target variable and one or more secondary variable (Chilès and Delfiner, 1999). Previous research has demonstrated that Cokriging can be used for downscaling and sharpening airborne raster data (Atkinson et al., 2008; Pardo-Igúzquiza et al., 2006). We extended the traditional Cokriging method from the spatial domain to the space-time domain to model the spatial, temporal, and spatio-temporal correlations in the LULC change process. The primary variable was the NLCD LULC images with low spatial resolution but high temporal frequency at multiple time points. The secondary co-variable was the high spatial resolution image acquired at one time point. The derived spatio-temporal Cokriging predictor can be expressed as:

$$\hat{Z}_\epsilon^{t_0}(s_0) = \sum_{i=1}^T \sum_{j=1}^N \alpha_{ij} Z_\epsilon^{t_i}(s_{ij}) + \sum_{k=1}^M \beta_k Z_v^{t_2}(u_k) \tag{1}$$

where $\hat{Z}_\epsilon^{t_0}(s_0)$ is spatio-temporal probability at location s_0 and time t_0 . $Z_\epsilon^{t_i}(s_{ij})$ is time-series LULC at pixel s_{ij} and time t_i ; $Z_v^{t_2}(u_k)$ is the high resolution secondary co-variable at location u_k and time t_2 . α_{ij} and β_k are two sets of weight to be estimated by minimizing the corresponding mean squared prediction error (Chilès and Delfiner, 1999). Mathematically, two sets of weights were obtained by solving the spatio-temporal covariance system, $C\lambda = b$, where

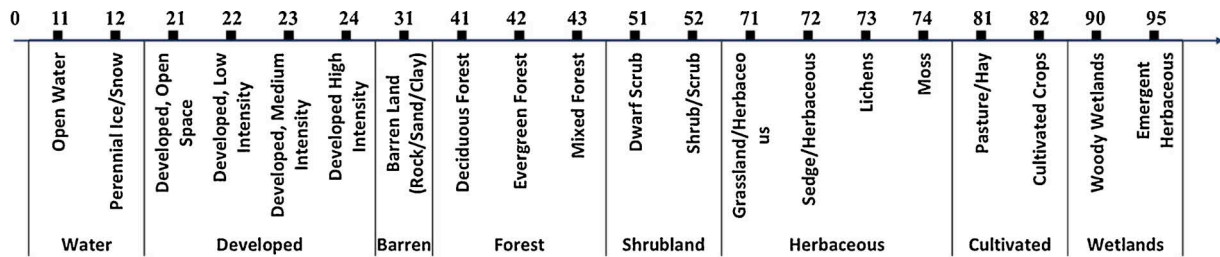


Fig. 1. Class numbers in the Anderson classification system.

$$C = \begin{bmatrix} C_1^{i1} & C_{12}^i & 1_{N_T} & 0_{N_T} \\ C_{21}^i & C_2 & 0_M & 1_M \\ 1_{N_T} & 0_M & 0 & 0 \\ 0_{N_T} & 1_M & 0 & 0 \end{bmatrix} \quad (2)$$

The spatio-temporal covariance matrix C has covariance C_1^{i1} , which is the $N_i \times N_i$ covariance matrix of the primary variable at time t . C_{12}^i is the $N_i \times M$ cross-covariance matrix between primary variable at time t_1 and the secondary co-variable at time t_2 with $C_{21}^i = C_{12}^{i'}$. C_2 is the $M \times M$ covariance matrix of the secondary variable at time t_2 .

In the right-side of the equation, $b = [C_1^i(s_0) \ 1 \ 0]'$, where $C_1^i(s_0)$ is the $N_i \times 1$ cross-covariance vector between primary variable at time t_i and predicting location s_0 , $C_2(s_0)$ is the $M \times 1$ cross-covariance vector between the secondary co-variable at time t_2 and the predicting location s_0 . $\lambda = [\alpha_{TN_T} \ \beta_M \ m_1 \ m_2]'$, where m_1 and m_2 are Lagrange multipliers (Myers and Milton, 1991) for the two constraints: $\sum_{i=1}^T \sum_{j=1}^{N_i} \alpha_{ij} = 1$; $\sum_{k=1}^M \beta_k = 0$. Solving the Cokriging system via the inversion of matrix C , we obtained the weights and the corresponding predictor $\hat{Z}_e^{t_0}(s_0)$. With varying s_0 over the spatial domain of interest and t_0 over the time domain, we obtained the prediction for the primary variable over time at the same spatial resolution as the secondary co-variable. This, therefore, generated the spatio-temporal sharpening imagery.

To satisfy the secondary-stationary assumption, a detrending process is required (Snepvangers et al., 2003). Here, a local mean value of pixels at the closest predicting time was estimated as the trend surface. The residuals after removing the fitted trend surface were used to estimate the semi-variogram and autocorrelations. In addition, in this study, as in general practice, (co)kriging was implemented locally within a moving window. The window's size was chosen based on the effective range of the spatial semi-variogram, since it indicates the valid spatial range of the spatial dependency.

2.3. Building the spatio-temporal structure

To estimate the spatio-temporal structure, we used the spatio-temporal covariance function governing both spatial and temporal covariance. But there are some challenges in constructing a model for the spatio-temporal semi-variogram. First, to be a valid covariance function, the function must satisfy a positive-definiteness condition (Cressie, 1993). A property of the spatio-temporal covariances is that they can be written as a product of a valid spatial covariance and a valid temporal covariance (De Cesare et al., 2001). While this product did not model the interaction (Cressie and Huang, 1999), it is computationally efficient for regular raster data and can ensure the positive-definiteness condition. Accordingly, we chose the spatial-temporal covariance function for achieving the best balance between efficiency and accuracy.

$$cov(Z_1(s_1, t_1), Z_2(s_2, t_2)) = cov_s(s_1 - s_2) \cdot r_t(t_1 - t_2) \quad (3)$$

where cov_s is the valid spatial covariance and r_t is the temporal correlation function. As in classical geostatistics and time-series analysis, we first used the available images to compute the empirical spatial semi-

variogram $\hat{\gamma}_s$ and empirical temporal semi-variogram $\hat{\gamma}_t$. Then, appropriate parametric spatial semi-variogram and auto correlation models were chosen. The ordinary least squares (OLS) adjustment fitting method was used in this case to estimate associated model parameters.

Spatial semi-variogram $\gamma_s(h_s)$ was computed by selecting pixel pairs with the spatial distance h_s , then their average squared differences were calculated by:

$$\gamma_s(h_s) = \frac{1}{2N(h_s)} \sum_{i=1}^{N(h_s)} [Z_1(s_1, t_1) - Z_2(s_1 + h_s, t_1)]^2 \quad (4)$$

where $N(h_s)$ is the number of randomly chosen pixel pairs. In this study, 5000 randomly chosen pairs of pixels with a spatial distance h_s were used to calculate the spatial semi-variogram and to estimate the spatio-temporal covariance structure as the training dataset.

Next, the empirical temporal semi-variogram $\gamma_t(h_t)$ was calculated as the function of the temporal distance h_t (in year). Time-series LULC images were used to calculate the temporal semi-variograms. Time-series data acquired in h_t years before or after the predicted time points were used in the following equation,

$$\gamma_t(h_t) = \frac{1}{2N(h_t)} \sum_{i=1}^{N(h_t)} [Z_1(s_1, t_1) - Z_2(s_1, t_1 + h_t)]^2 \quad (5)$$

where $N(h_t)$ is the number of pixel pairs which are located at the same location while separated by h_t years.

Both spatial and temporal semi-variograms are required to estimate the covariance matrix. We constructed the empirical variograms based on the available LULC data, since Anderson classification system coded the more related classes with closer numbers. The spatial semi-variogram was estimated using high resolution data with more detailed spatial information. Meanwhile, the temporal semi-variogram was estimated by using the time-series primary variable, because there was only one frame of the secondary variable available in the temporal domain and that time point was included in the temporal domain of the primary variable. As the spatial and the temporal semi-variograms were estimated from different dataset, the change-of-support was not involved in the calculation in this study.

3. Study area and data acquisition

3.1. Study area

The upper portion of the Mill Creek watershed (UMCW) in southwestern Ohio (Fig. 2) was selected to demonstrate the LULC sharpening results through ST-Cokriging. Mill Creek is 72.4 km long, stretching from its headwater in the eastern central part of Butler County through the industrial centers of the Hamilton County before it joins the Ohio River in the western side of downtown Cincinnati. Because of its location, the Mill Creek Valley has been serving as a transportation corridor for industrial development and has helped to build Cincinnati into a prosperous industrial powerhouse (Mill Creek Watershed Council, 2017). Over the years, the UMCW has been experiencing rapid urbanization. Its population has doubled in the last 20 years to nearly 40,000 (U.S. Census Bureau, 2014), and its land use has been changing

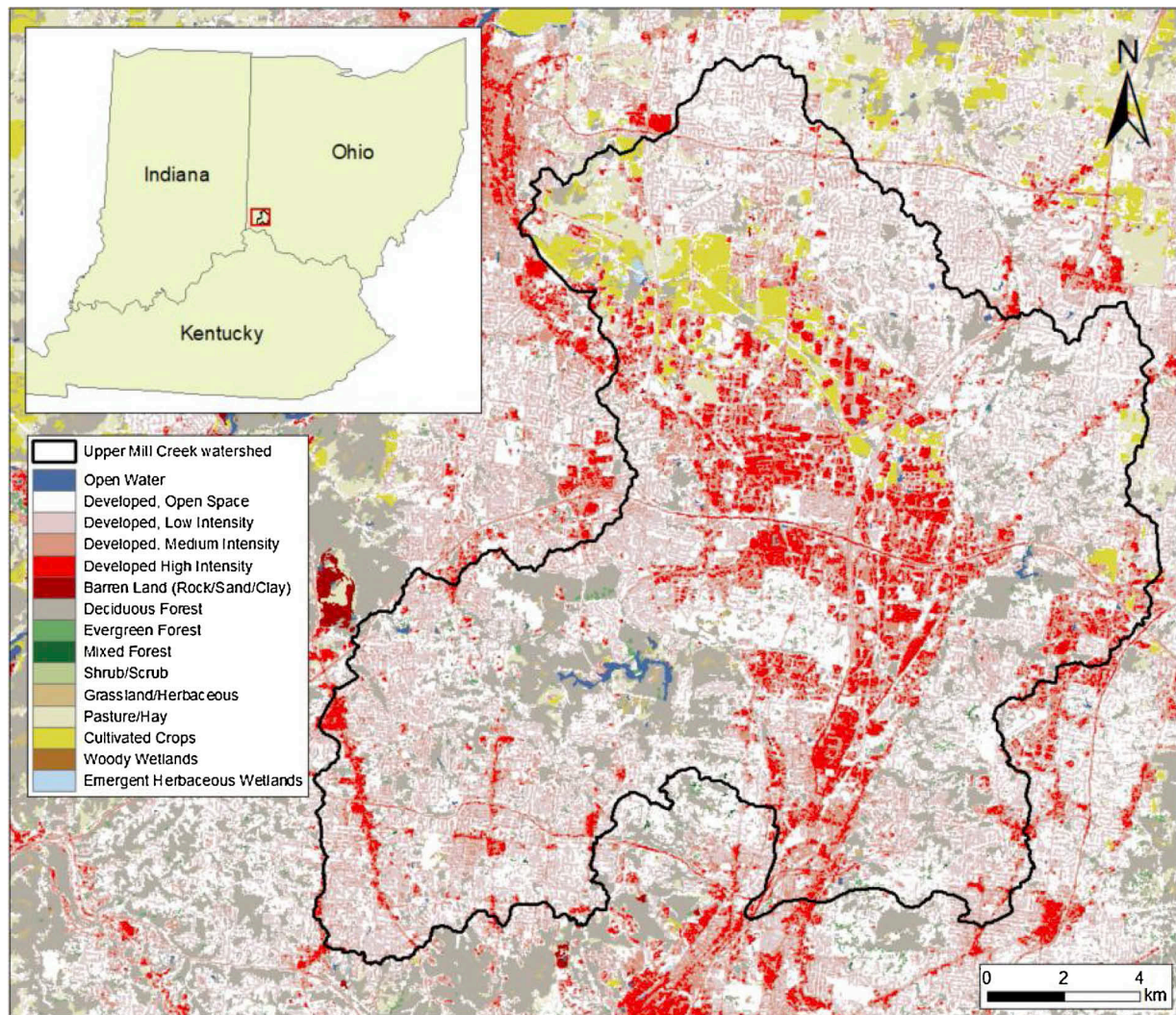


Fig. 2. The UMCW overlay with 2011 NLCD LULC data.

rapidly, especially in and around Liberty Township in the southeastern region of Butler County along the interstate I-75. As the UMCW continues to be developed, there will be more changes in its already heterogeneous and diversified LULC. The UMCW is therefore an ideal study area to demonstrate the efficacy of spatio-temporal modelling and LULC data sharpening.

3.2. LULC data as the primary variable

All LULC images were clipped to the UMCW and projected to NAD 1983 State Plane Ohio South FIPS 3402 coordinate system. Fig. 3 shows the 1992, 2001, 2006, and 2011 NLCD LULC over the UMCW. It is evident that since 1992, the overall LULC trend of the area is a decrease of vegetation coverage. The developed regions with class codes of 20 to 25 expanded from 232.6 km² in 2001 to 239.1 km² in 2006 and 240.1 km² in 2011.

Since the original 1992 NLCD LULC map was generated from unsupervised classification of Landsat Thematic Mapper (TM) circa 1990's satellite data (Riitters et al., 2002), it has a different legend from the other maps. Hence, we did not directly compare the 1992 data with other NLCD data; instead, they were used as supporting data to estimate the spatio-temporal structure.

One challenge in estimating the spatio-temporal LULC changes is the lack of temporal valid points and the relatively short sampling period. To better depict the spatio-temporal LULC changes, we need

multiple land use measurements covering an extensive temporal domain to provide additional information of the temporal structure and a longer temporal trend of LULC change. To circumvent this requirement, we generated future LULC scenarios for 2030, 2040, and 2050 using a Markov Cellular Automata (CA-Markov) model in IDRISI (Clack Labs, 2012). The predictability of the LULC map generated from IDRISI was verified by comparing the simulated 2011 map with the actual 2011 NLCD map using Kappa statistic, a commonly used measure of the overall accuracy of agreement between two images (Pontius et al., 2001). It has a value ranging from 0 (no agreement between the two images) to 1 (perfect agreement). Because the value of the Kappa statistic in this research was found to be 0.9291, the model results were accepted and coded in accordance with the Anderson Level II classification criteria. The “urban areas” in the future land use scenarios were classified into “developed open space,” “developed low intensity,” “developed medium intensity,” and “developed high intensity” (Fig. 4).

Modeling results show that the total areal extent of developed regions with class codes 20 to 25 expanded from 202.4 km² in 2030 to 202.8 km² in 2040 and 207.2 km² in 2050. While all of these four categories depict urbanized lands, the speed of impervious surface expansion in each category is different.

3.3. Airborne imagery and object-oriented classification

The Ohio government has deployed two airborne imagery

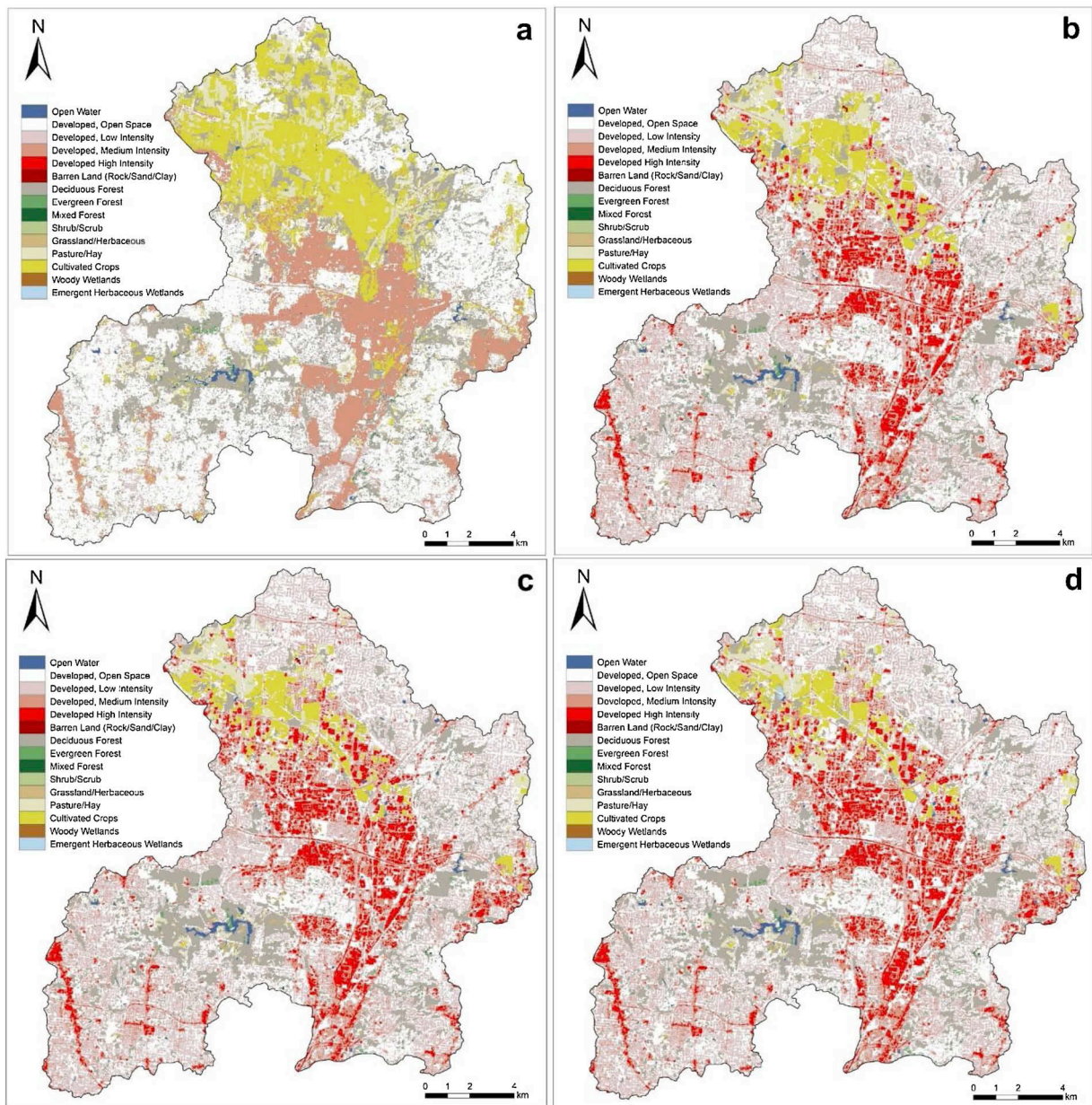


Fig. 3. NLCD LULC over the UMCW in a) 1992; b) 2001, c) 2006, d) 2011.

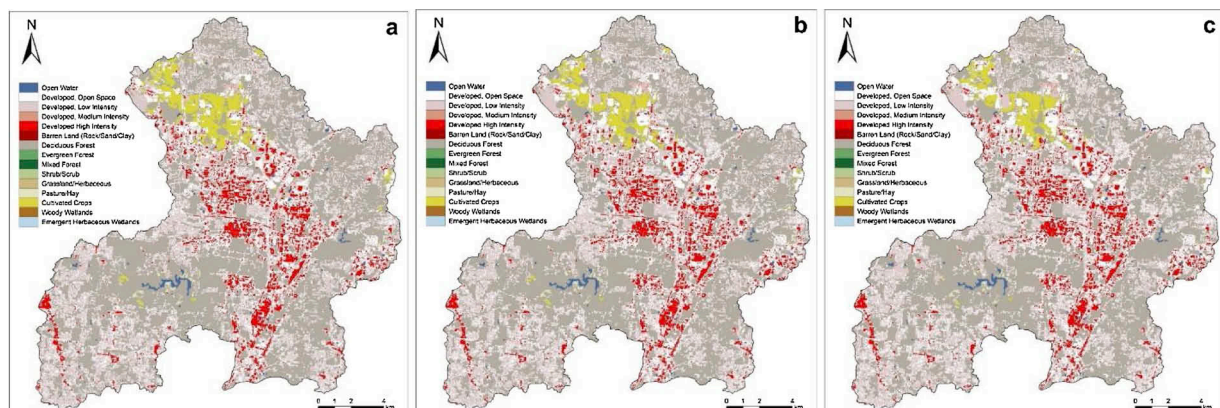


Fig. 4. IDRISI simulated LULC patterns over the UMCW in: a) 2030; b) 2040, c) 2050.

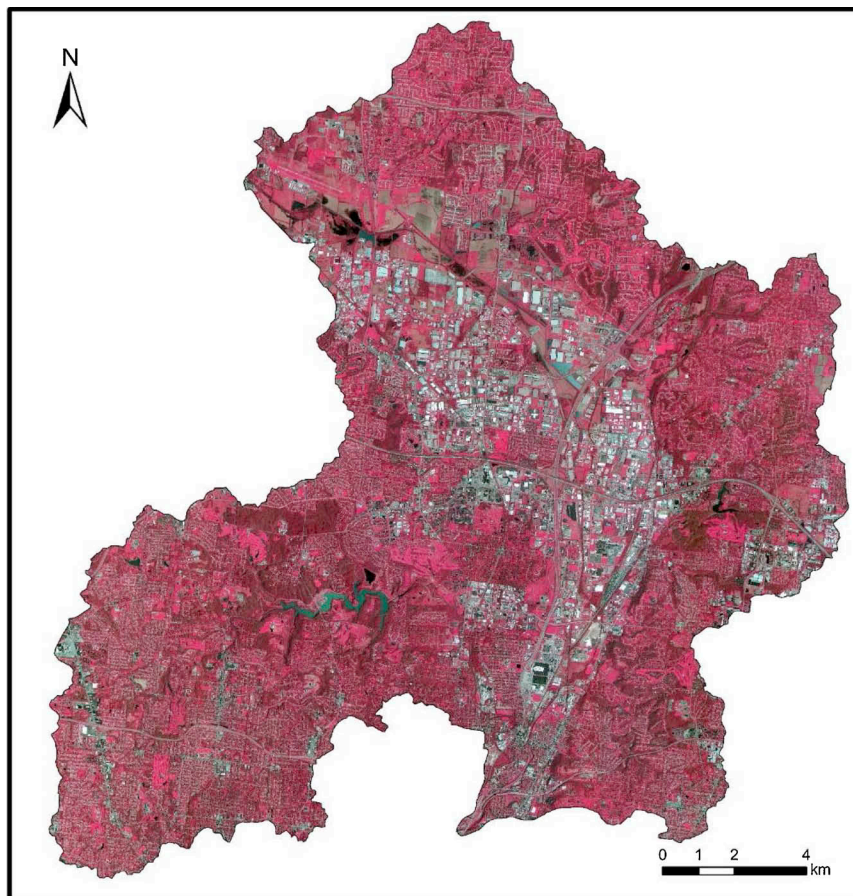


Fig. 5. 2007 OSIP I airborne imagery over the UMCW with NIR false color combination at a 3-m resolution.

reconnaissance surveys, one in 2007–2008 (OSIP I) and the other in 2010–2011 (OSIP II), to acquire high spatial resolution (3 m or less) airborne imagery. In this study, we used the 2007 OSIP I as the co-variable for ST-Cokriging sharpening and the 2011 OSIP II imagery for validating the sharpening results. The 2007 OSIP I imagery has near infrared (NIR), red, and green bands (Fig. 5). Ground control points were collected by the OSIP airborne imagery survey group to geo-register the airborne imagery and validate the imagery. According to OGRIP (2017), the overall accuracy of the imagery product is within 0.0254 m.

We used object-oriented classification method to classify the high resolution OSIP airborne images to the Anderson classification system. When compared with the pixel-based classification, object-oriented classification is better suited to extract land use objects, such as buildings, and its results have better clarity and more contiguous shapes. With appropriate training samples and parameters, the method has an excellent capability to delineate objects at a local scale (Jacquin et al., 2008). It is therefore widely used for automatic and semi-automatic LULC classification in urban areas (Liu et al., 2010; Zhang et al., 2014).

The object-oriented classification on the OSIP high resolution airborne imagery was performed using eCognition (Trimble, 2017). To illustrate the results of our analyses in more detail, we chose an area near Liberty Township, the fastest growing area in the UMCW with rapid LULC changes, as a zoomed-in enlarged area (Fig. 6). Multi-resolution classification was used because the high resolution airborne imagery contains NIR, red, and green bands. To obtain the best classification results, we set the object size to 200, which was the average number of pixels for objects in the study region. To calibrate the classification parameters, a sample of classification results was compared to the NLCD 2006 LULC data (the selected training object shown in Fig. 6b

and c). By adjusting the coefficients of the shape and compactness of the image objects to 0.1 and 0.5 respectively, a new LULC map with a finer spatial resolution (3 m) was produced (Fig. 6a and d). For validation of the classification results, we used some easily identifiable targets, such as water bodies, on the image. Ground truth validation ascertains that these targets are well delineated in our classification results; they are more distinct, clearly discernable, and with better shapes.

4. Results and discussion

4.1. Estimation of ST-Cokriging equations

The first step of ST-Cokriging was to estimate the spatio-temporal covariance structure using a primary variable (the time-series NLCD LULC data with a 30-m spatial resolution) and a secondary variable (the one frame of OSIP I LULC airborne imagery with a 3-m spatial resolution). The results of estimated spatial and temporal empirical semi-variograms derived from Eqs. (4) and (5) are shown in Figs. 7a and b.

The exponential function was chosen to model both the spatial and temporal semi-variograms and to characterize the covariance structures because it provided the best fit to the empirical semi-variograms. Specifically:

$$\gamma_s(h_s) = 219 \cdot [1 - \exp(-\frac{h_s}{194.4})] \quad (6)$$

and:

$$\gamma_t(h_t) = 348 \cdot [1 - \exp(-\frac{h_t}{14.4})] \quad (7)$$

As shown in Fig. 7a and b, the sill values, which represent the spatial/temporal variances of the variable, are 219 and 348 for the

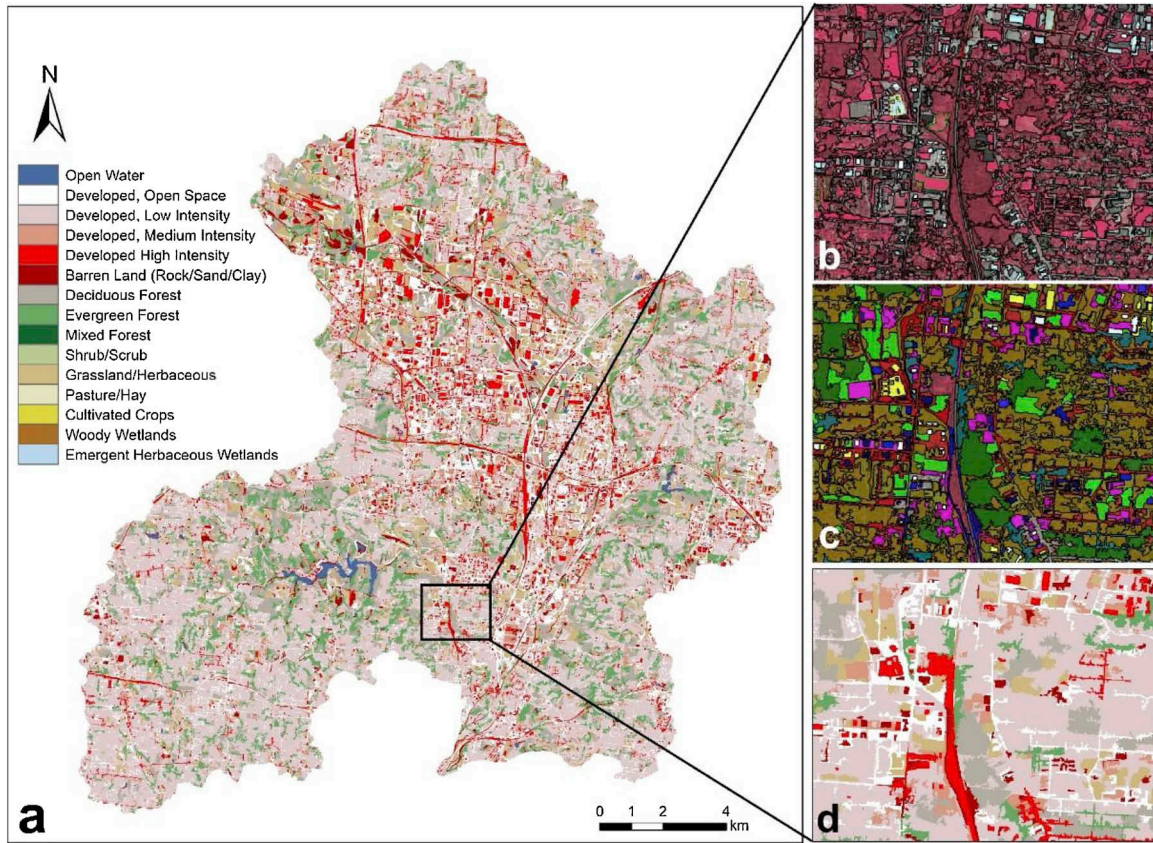


Fig. 6. a) Object-oriented classification results for the 2007 OSIP I airborne image over the UMCW, b) NIR false color combination imagery for an enlarged area (near Liberty Township) of the study region, c) training data objects for the object-oriented classification over the same area, and d) object-oriented classification results over the same area.

spatial and temporal models, respectively. According to Cressie (1993), the effective range is the distance at which the semi-variance reaches 95% of the sill. In this research, the spatial effective range value is 583.2m and temporal effective range is 43.2 years. Because we were modeling the LULC change over a long period, the measurement error (nugget effect) are considered to be infinitesimal in the variogram fitting (Kang et al., 2009).

4.2. Sharpening results and validation

To test and validate the spatio-temporal sharpening performance of the Cokriging algorithm, we used the 2001, 2006, and 2011 NLCD LULC data and the high resolution 2007 object orientation classification results of the OSIP I airborne image as the source data and applied the ST-Cokriging

algorithm to generate a sharpened LULC map of 2011 at a 3-m spatial resolution. Fig. 8 shows the results of the validation. Here, we included the 2011 NLCD LULC map (Fig. 8a) to illustrate the coarse resolution source data. We also included the results of the enlarged area near Liberty Township to highlight the sharpening result from ST-Cokriging. Fig. 8b shows the secondary co-variable of OSIP I airborne imagery classification results. From the figures, it is unequivocal that the airborne imagery classification result (Fig. 8b) has more detail information, and it can depict the spatial pattern more clearly than the NLCD LULC data.

Fig. 8c is the sharpened 2011 LULC probability map at a 3-m spatial resolution calculated by the ST-Cokriging algorithm. From the spatio-temporal structure, the probability value of each pixel was generated, which represents the probability of change between the two adjacent class codes in the spatio-temporal domain of the LULC trend.

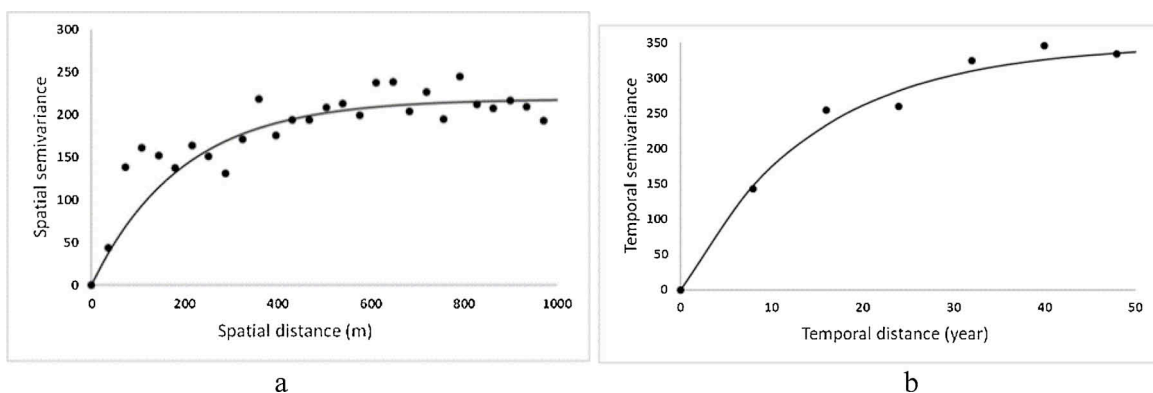


Fig. 7. a) Spatial semi-variogram and exponential fitting model, b) Temporal semi-variogram and exponential fitting model.

The LULC probability map was converted to Anderson classification LULC map using the nearest neighbor approach (Fig. 8d). For validation, the sharpening results were compared with the 2011 OSIP II airborne image using the K-fold cross-validation method, where the original sample was randomly divided into K equal subsamples to reduce overfitting. With this method, each observation is used to validate the model only once and train the model k-1 times. Here, K was set to 10 to cross-validate the sharpening performance. Apart from the 5000 pixels that we selected as the training dataset to estimate the spatio-temporal structure, another 5000 points were randomly selected to calculate the confusion matrix and Kappa value, and we repeated the calculation 10 times. When the 2011 sharpening results were compared with the OSIP

II data, the 10-fold average value of the Kappa score was 0.9385. In the enlarged region of Liberty Township, it clearly shows that detailed spatial LULC pattern has been extracted from the sharpening results. Roads, greenbelts, boundaries of buildings and farmlands are much clearer than that shown under the coarse resolution source data (Fig. 8a). The generated LULC pattern was found to be in accordance to the reference image.

4.3. Estimating LULC changes on sharpened time-series maps

We used the high resolution airborne LULC map and the 1992 and 2001 NLCD maps to generate the sharpened map for 2001; the 1992,

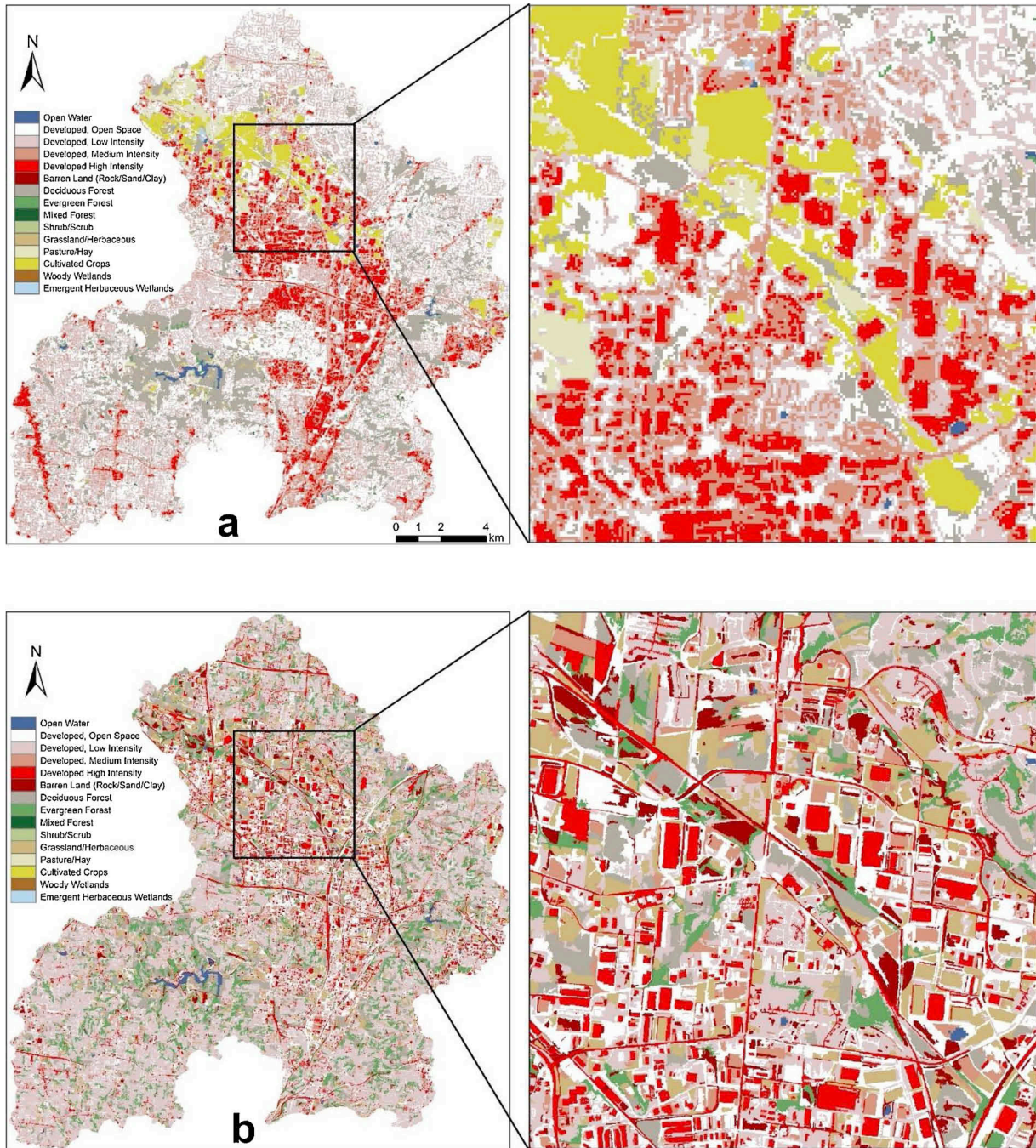


Fig. 8. ST-Cokriging sharpening results: a) NLCD LULC map in 2011 at 30-m resolution and the enlarged area; b) 2007 OSIP I airborne image classification results at 3-m resolution and the enlarged area; c) ST-Cokriging sharpened LULC probability map at 3-m resolution in 2011 and the enlarged area; d) ST-Cokriging LULC map using Anderson classification system at 3-m resolution and the enlarged area.

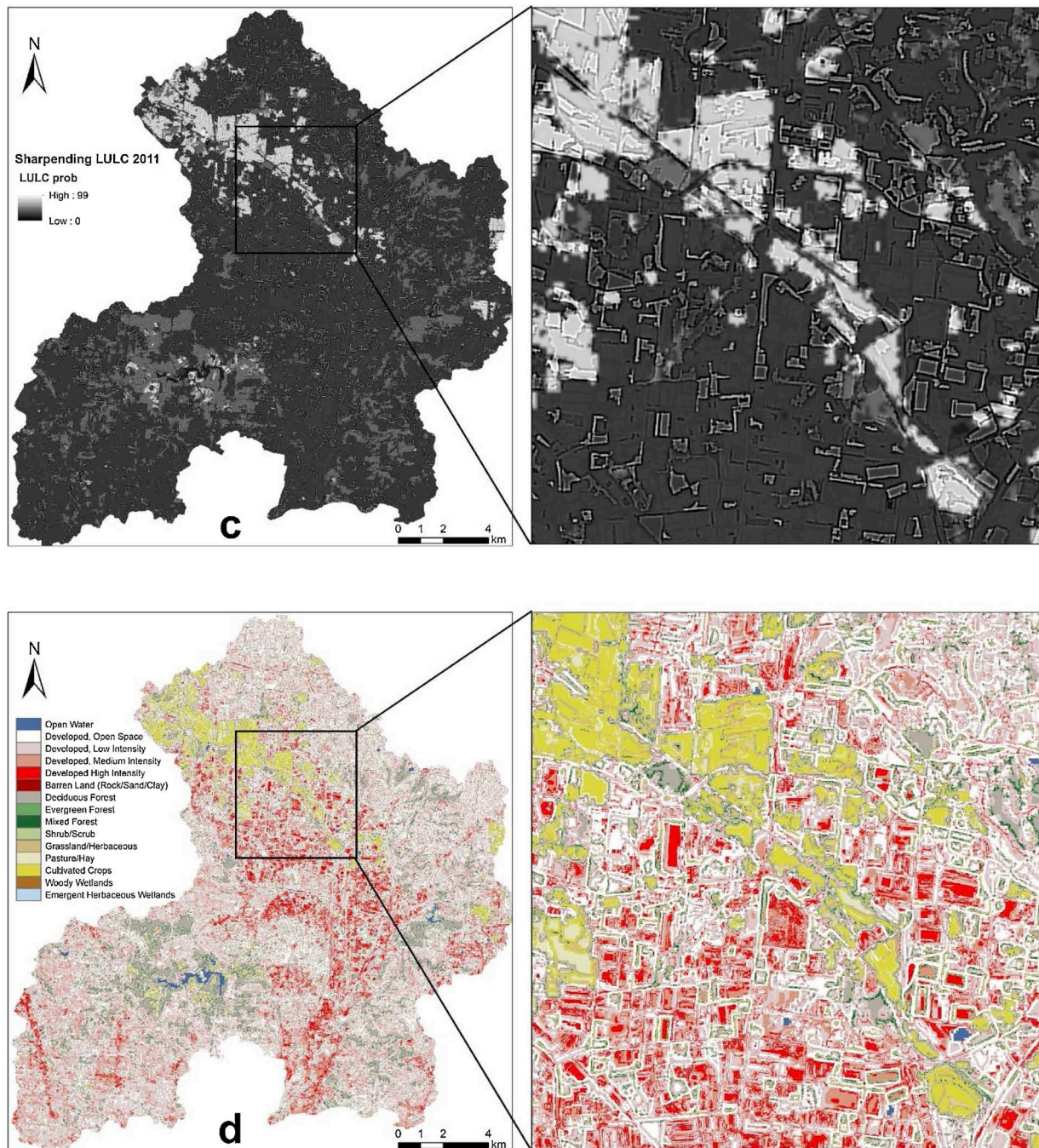


Fig. 8. (continued)

2001, 2006 NLCD maps to generate the sharpened map for 2006; and the 2001, 2006, 2011 NLCD maps to generate the sharpened map of 2011. Together, we created a time-series ST-Cokriging sharpened LULC maps at 3 m over the UMCW (Fig. 9).

To highlight the utility of the sharpened high resolution map in LULC change detection, two maps of LULC change of the enlarged area were also created. Fig. 10 shows the changes from 2001 to 2006 and from 2006 to 2011. They were coded according to the LULC values on the sharpened high resolution LULC maps and were divided into five categories based on the class codes and class probabilities:

- Built-up area – the LULC class code value is within the category of developed land (Anderson classification code 21–24), or the class probability of LULC change shows that it will mostly remain within the developed land category. It represents the built-up area or an

area under reconstruction from a previously developed area.

- Crop/grass to built-up area – the change of the LULC value is from cropland (Anderson classification code 81–82) or grassland (71–74) to developed land. It represents the newly reclaimed impervious surface converted from agricultural land.
- Forest to built-up area – the change of the LULC value is from forest (Anderson classification code 41–43 or 51–52) to developed land. It represents the newly deforested area changing from forested to developed area.
- Built-up to vegetated area – the change of the LULC value is from developed area to vegetated surfaces (Anderson classification code 41–82). It represents the area of impervious surface changing back to vegetated area.
- No change area – there is no substantial change on the LULC probability map.

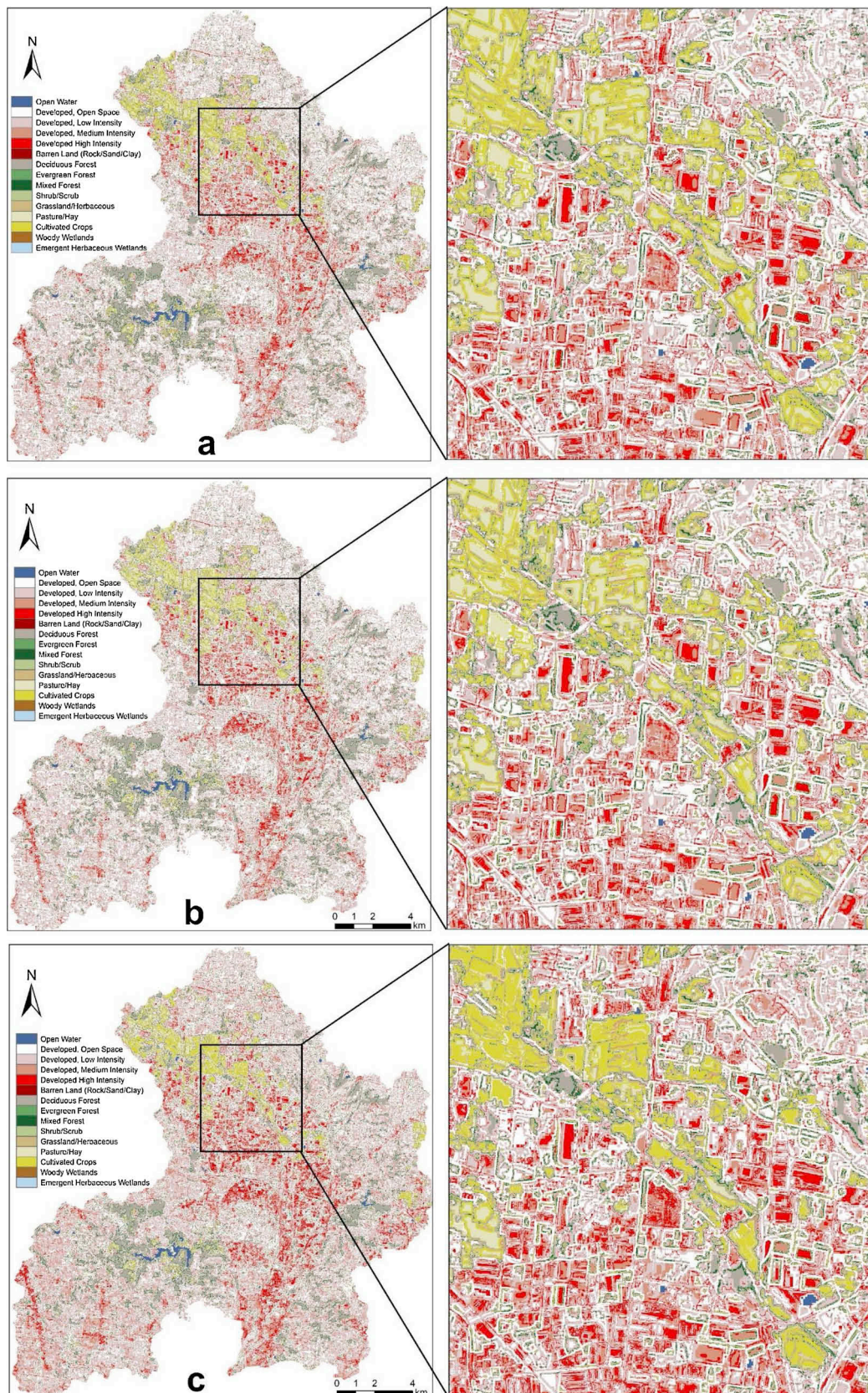


Fig. 9. Sharpened high resolution LULC maps derived from ST-Cokriging for a) 2001, b) 2006, and c) 2011 at a 3-m spatial resolution over the UMCW and the enlarged area near Liberty Township.

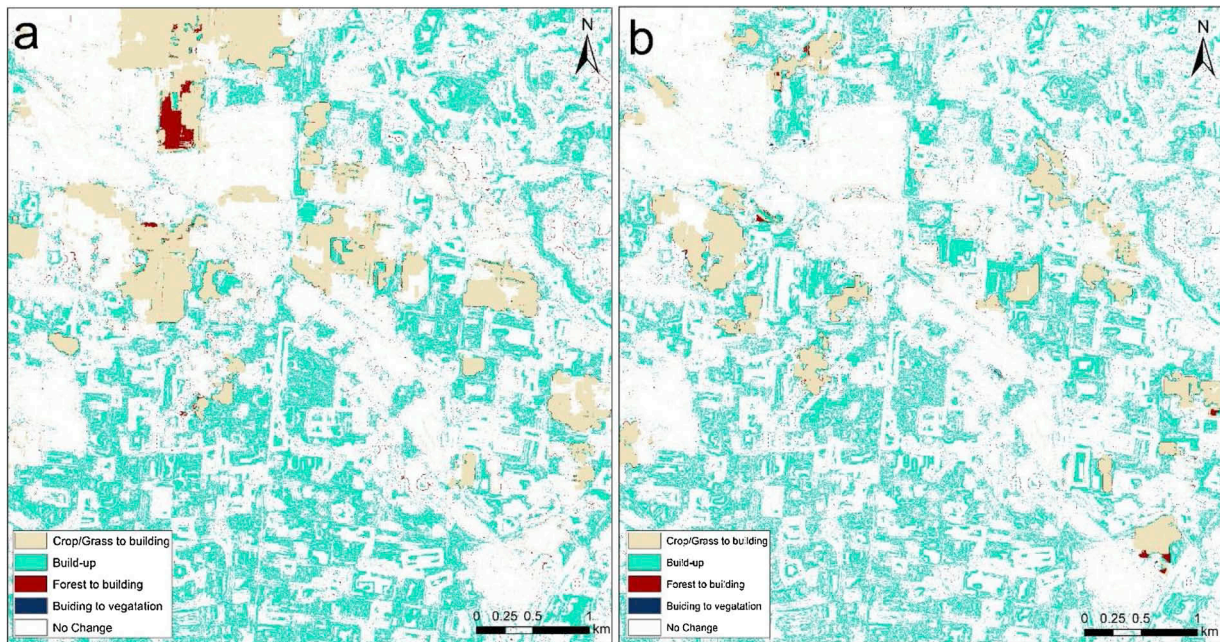


Fig. 10. An enlarged part of land use change near Liberty Township, a) from 2001 to 2006, b) from 2006 to 2011.

Table 2

LULC change (in km²) for the UMCW from 2001 to 2006 and 2006 to 2011.

Class	Change of LULC code	2001–2006	2006–2011
Built-up area	21–24 to 21–24	82.06 km ²	62.07 km ²
Crop/grass to building area	71–82 to 21–24	7.28 km ²	4.54 km ²
Forest to building area	41–52 to 21–24	2.54 km ²	0.34 km ²
Built-up to vegetation area	21–24 to 41–82	0.02 km ²	1.56 km ²

Table 2 shows the area under each LULC change category in the UMCW. While it is evident that the region is undergoing a very pronounced urbanization process from 2001 to 2011, the sharpened high resolution LULC maps from ST-Cokriging reveal more details of the LULC change. Fig. 10 shows that from 2001 to 2006 and from 2006 to 2011, a vast portion of Liberty Township changed from vegetated area to developed area. Most of the impervious surface areas were developed from the crop/grass area, but a large portion of the forested lands could still be found surrounding the developed areas. This may be because it is more cost-effective to convert the crop/grass (rather than forested) areas to impervious areas. Fig. 10b shows that most of the newly urbanizing areas were found in the marginal areas bordering the original urbanized areas as depicted in Fig. 10a. However, the areal extent of this area was smaller than that in Fig. 10a. It can be inferred that the majority of the urbanization process started during the period from 2001 to 2006, where many land parcels had been reclaimed and cleared for development. For the subsequent five-year period, from 2006 to 2011, many of these open spaces were developed and were replaced by the newly constructed buildings and impervious surfaces. Although there was a huge portion of vegetated area changing to developed area, only a very small area of impervious surface and a few buildings were converted back to vegetated area, often as newly planted trees surrounding the developed areas. The predominant change in LULC was therefore an increase in built-up areas; most of which was converted from reclaimed vegetated areas while some lower intensity developed areas were also converted to higher intensity development. From this analysis, it is apparent that the shape of the sharpened image and the relative position of the changes of LULC can offer useful insights into the trend of LULC change over time; as such, better inferences can be drawn.

5. Conclusions

This paper presents a geostatistical approach of spatio-temporal sharpening of LULC data. Our ST-Cokriging algorithm extended the traditional Cokriging method from a spatial domain to a spatio-temporal domain by modelling spatial covariance, temporal covariance, and spatio-temporal covariance. By taking advantage of airborne imagery as a secondary co-variable, it can spatially sharpen the time-series LULC maps to higher spatial resolution while temporally estimate the trend probability map, thereby revealing the changing direction and speed quantitatively.

Previous LULC sharpening methods were primarily based on investigating the spectral patterns and decomposing the pixel nesting structure, and few of them established the quantitative connection and transmission between LULC classes. We utilized the Anderson classification system to ensure that the LULC classes can be calculated and transmitted through ST-Cokriging sharpening. Using the ST-Cokriging algorithm on the LULC data over the UMCW at a 30-m spatial resolution, we generated the sharpened LULC at a 3-m spatial resolution as well as a set of probabilities for LULC change. The algorithm has been successfully applied to sharpen the historical and future LULC data. The results demonstrate that our method can effectively generate reliable results with detailed LULC features and enhance the interpretation and extraction of surface features.

From our sharpened LULC maps, it is obvious that the shapes of the land use and spatial nest relations are more readily identifiable. The new maps provide more detail characterizations and accurate estimations of LULC change. By showing how the expansion of the “open space developed land” is alternating with the growth of developed lands, the new maps help to reveal a clearer picture of the urbanization process. By quantitatively measuring the probabilities of LULC change between land use classes, the sharpened LULC probability maps also help us to understand further the trend of land use change. Better quality time-series land use data can also help us to differentiate the variabilities of changes within one land use category over time.

Declaration of interests

None.

References

- Anderson, J.R., Hardy, E.E., Roach, J.T., Witmer, R.E., 1976. A land use and land cover classification system for use with remote sensor data. Geological Survey Professional Paper 964. U.S. Geological Survey, Alexandria, VA (Accessed 15 November 2017). <https://pubs.usgs.gov/pp/0964/report.pdf>.
- Atkinson, P.M., Pardo-Igúzquiza, E., Chica-Olmo, M., 2008. Downscaling Cokriging for super-resolution mapping of continua in remotely sensed images. *IEEE Trans. Geosci. Remote. Sens.* 46 (2), 573–580. <https://doi.org/10.1109/TGRS.2007.909952>.
- Chilès, J., Delfiner, P., 1999. *Geostatistics: Modeling Spatial Uncertainties*, second edition. Wiley, New York.
- Clark Labs, 2012. IDRISI GIS Analysis. (Accessed 29 March 2016). <https://clarklabs.org/>.
- Cressie, N., 1993. *Statistics for spatial data*. Wiley Series in Probability and Mathematical Statistics. Wiley <https://doi.org/10.1002/9781119115151>. (Accessed 15 November 2017).
- Cressie, N., Huang, H.C., 1999. Classes of nonseparable, spatio-temporal stationary covariance functions. *J. Am. Stat. Assoc.* 94 (448), 1330–1339. <https://doi.org/10.2307/2669946>.
- De Cesare, L., Myers, D.E., Posada, D., 2001. Estimating and modeling space–time correlation structures. *Stat. Probab. Lett.* 51 (1), 9–14.
- Fan, R., Tong, S.T.Y., Lee, J.G., 2017. Determining the optimal BMP arrangement under current and future climate regimes: case study. *J. Water Resour. Plan. Manag.* 143 (9), 1–15. [https://doi.org/10.1061/\(ASCE\)WR.1943-5452.0000816](https://doi.org/10.1061/(ASCE)WR.1943-5452.0000816).
- Gilbertson, J.K., Kemp, J., Van Niekerk, A., 2017. Effect of pan-sharpening multi-temporal Landsat 8 imagery for crop type differentiation using different classification techniques. *Comput. Electron. Agric.* 134, 151–159.
- Grigg, D., 1965. The logic of regional system. *Ann. Assoc. Am. Geogr.* 55 (3), 465–491. <https://doi.org/10.1111/j.1467-8306.1965.tb00529.x>.
- Jacquin, A., Misakova, L., Gay, M., 2008. A hybrid object-based classification approach for mapping urban sprawl in periurban environment. *Landsc. Urban Plan.* 84 (2), 152–165. <https://doi.org/10.1016/j.landurbplan.2007.07.006>.
- Jeganathan, C., Hamm, N.A.S., Mukherjee, S., Atkinson, P.M., Raju, P.L.N., Dadhwal, V.K., 2011. Evaluating a thermal image sharpening model over a mixed agricultural landscape in India. *Int. J. Appl. Earth Obs. Geoinf.* 13 (2), 178–191.
- Kang, E.L., Liu, D., Cressie, N., 2009. Statistical analysis of small-area data based on independence, spatial, non-hierarchical, and hierarchical models. *Comput. Stat. Data Anal.* 53 (8), 3016–3032. <https://doi.org/10.1016/j.csda.2008.07.033>.
- Kyriakidis, P.C., Journel, A.G., 1999. Geostatistical space–time models: a review. *Math. Geol.* 31 (6), 651–684. <https://doi.org/10.1023/A:1007528426688>.
- Ling, F., Manolakis, D., Proakis, J., 1986. A recursive modified Gram-Schmidt algorithm for least-squares estimation. *IEEE T. Acoust. Speech* 34 (4), 829–836. <https://doi.org/10.1109/TASSP.1986.1164877>.
- Liu, H., Wang, L., Sherman, D., Gao, Y., Wu, Q., 2010. An object-based conceptual framework and computational method for representing and analyzing coastal morphological changes. *Int. J. Geogr. Inf. Sci.* 24 (7), 1015–1041. <https://doi.org/10.1080/13658810903270569>.
- Liu, Y., Wang, L., Long, H., 2008. Spatio-temporal analysis of land use conversion in the eastern coastal China during 1996–2005. *J. Geogr. Sci.* 18 (3), 274–282. <https://doi.org/10.1007/s11442-008-0274-3>.
- Mill Creek Watershed Council, 2017. Know the Mill Creek. (Accessed 1 August 2017). <http://www.millcreekwatershed.org/whatiswatershed/>.
- MRLC (Multi-Resolution Land Characteristics Consortium), 2017. National Landcover Database. [dataset]. <https://www.mrlc.gov/> (Accessed 21 March 2017).
- Myers, R., Milton, J., 1991. *A First Course in the Theory of Linear Statistical Models*. PWS-KENT Pub. Co., Boston.
- OGRIP, 2017. OGRIP (Ohio Geographically Referenced Information Program). [dataset]. <http://ogrip.oit.ohio.gov/> (Accessed 20 April 2017).
- Pardo-Igúzquiza, E., Chica-Olmo, M., Atkinson, P.M., 2006. Downscaling Cokriging for image sharpening. *Remote Sens. Environ.* 102 (1–2), 86–98. <https://doi.org/10.1016/j.rse.2006.02.014>.
- Pontius, R.G., Cornell, J.D., Hall, C.A., 2001. Modeling the spatial pattern of land use change with GEOMOD2: application and validation for Costa Rica. *Agric. Ecosyst. Environ.* 85 (1–3), 191–203. [https://doi.org/10.1016/S0167-8809\(01\)00183-9](https://doi.org/10.1016/S0167-8809(01)00183-9).
- Riitters, K.H., Wickham, J.D., O'Neill, R.V., Jones, K.B., Smith, E.R., Coulston, J.W., Wade, T.G., Smith, J.H., 2002. Fragmentation of continental United States forests. *Ecosystems* 5 (8), 815–822. <https://doi.org/10.1007/s10021-002-0209-2>.
- Snepvangers, J.J.J.C., Heuvelink, G.B.M., Huisman, J.A., 2003. Soil water content interpolation using spatio-temporal kriging with external drift. *Geoderma* 112 (3–4), 253–271. [https://doi.org/10.1016/S0016-7061\(02\)00310-5](https://doi.org/10.1016/S0016-7061(02)00310-5).
- Sun, Y., Tong, S., Yang, Y.J., 2016. Modeling the cost-effectiveness of stormwater best management practices in an urban watershed in Las Vegas Valley. *Appl. Geogr.* 76, 49–61. <https://doi.org/10.1016/j.apgeog.2016.09.005>.
- Tong, S.T.Y., Naramngam, S., 2007. Modeling the impacts of farming practices on water quality in the Little Miami River Basin. *Environ. Manage.* 39 (6), 853–866. <https://doi.org/10.1007/s00267-006-0307-6>.
- Trimble, 2017. *Ecognition Software*. (Accessed 21 July 2017). <http://www.ecognition.com/essentials>.
- U.S. Census Bureau, 2014. Data Release. [dataset]. <https://www.census.gov/programs-surveys/acs/news/data-releases/2014.html> (Accessed 21 December 2014).
- van der Sande, C.J., de Jong, S.M., de Roo, A.P.J., 2003. A segmentation and classification approach of IKONOS-2 imagery for land cover mapping to assist flood risk and flood damage assessment. *Int. J. Appl. Earth Obs. Geoinf.* 4 (3), 217–229. [https://doi.org/10.1016/S0303-2434\(03\)00003-5](https://doi.org/10.1016/S0303-2434(03)00003-5).
- Verhoeve, J., Wulf, R.D., 2002. Land cover mapping at sub-pixel scales using linear optimization techniques. *Remote Sens. Environ.* 79 (1), 96–104. [https://doi.org/10.1016/S0034-4257\(01\)00242-5](https://doi.org/10.1016/S0034-4257(01)00242-5).
- Yocky, D., 1996. Multiresolution wavelet decomposition image merger of Landsat thematic mapper and SPOT panchromatic data. *Photogramm. Eng. Remote Sensing* 62 (9), 1067–1074.
- Zhang, Q., Liu, C., Zhang, G., Zhou, A., 2014. Adaptive image segmentation by using mean-shift and evolutionary optimisation. *IET Image Process.* 8 (6), 327–333. <https://doi.org/10.1049/iet-ipr.2013.0195>.